Magic Wavelength to Make Optical Lattice Clocks Insensitive to Atomic Motion

Hidetoshi Katori and Koji Hashiguchi

Department of Applied Physics, Graduate School of Engineering, The University of Tokyo, Bunkyo-ku, Tokyo 113-8656, Japan and CREST, Japan Science and Technology Agency, 4-1-8 Honcho Kawaguchi, Saitama 332-0012, Japan

E. Yu. Il'inova and V. D. Ovsiannikov

Physics Department, Voronezh State University, Universitetskaya ploschad 1, Voronezh 394006, Russia

(Received 1 May 2009; published 9 October 2009)

In a standing wave of light, a difference in spatial distributions of multipolar atom-field interactions may introduce atomic-motion dependent clock uncertainties in optical lattice clocks. We show that the magic wavelength can be defined so as to eliminate the spatial mismatch in electric dipole, magnetic dipole, and electric quadrupole interactions for specific combinations of standing waves by allowing a spatially constant light shift arising from the latter two interactions. Experimental prospects of such lattices used with a blue magic wavelength are discussed.

DOI: 10.1103/PhysRevLett.103.153004 PACS numbers: 37.10.Jk, 32.10.Dk, 32.80.Qk, 32.80.Rm

Quantum absorbers trapped in well-designed electromagnetic fields are the excellent candidates for future optical atomic clocks projecting uncertainties below 10^{-18} [1,2], which represent the state of the art of the precision spectroscopy [3,4]. While these atom traps provide long interrogation time and the Lamb-Dicke confinement of atoms necessary for ultrahigh resolution spectroscopy, the relevant trapping fields impose an inherent fundamental limit on measurement uncertainties due to the atomic multipolar [1,5–7] and hyperpolarizability effects [2,8]. It is of note that the detection and control [9–11] of the electric quadrupole interactions of ions with their trapping fields triggered an essential breakthrough for ion clocks operating on the S-D clock transitions to achieve the uncertainties of 10^{-15} and even below [3,12].

Recently, it was pointed out that the multipolar interactions of atoms with optical lattices may introduce a spatial mismatch of the lattice potentials in the clock transition, thus affecting the optical lattice clocks' uncertainties at 10^{-16} [13]. This inferred the slight breakdown of the original concept of the magic wavelength that cancels out the quadratic light shift in the clock transitions [2]. In this Letter, we discuss strategies to minimize the light shift uncertainties in optical lattice clocks by considering the electric dipole ($E1$), magnetic dipole ($M1$), and electric quadrupole ($E2$) interactions of atoms in a standing wave. For specific lattice geometries, we show that the magic frequency ω_m of a lattice clock can be defined so as to eliminate the spatial mismatch of the lattice potentials by allowing a spatially constant differential light shift that can be evaluated down to 10^{-18}. Consequently, optical lattice clocks free from atomic-motion-dependent clock shift are realized. We discuss experimental prospects for the ${}^1S_0 - {}^3P_0$ clock transition of Sr atoms. In particular, combined with a blue-detuned magic wavelength [14], the proposed lattice geometry closely simulates the Paul trap employed in ion clocks [1], thus pushing the lattice clocks' uncertainty towards the 10^{-18} regime.

Optical lattices consist of a spatially periodic light shift formed by an interference pattern of electromagnetic (EM) waves. The simplest configuration is a one-dimensional (1D) lattice created by a standing wave that can be taken to be $\mathbf{E} = \mathbf{e}_z E_0 \sin ky \cos\omega t$ with frequency ω and wave number $k = \omega/c = 2\pi/\lambda$ as shown in Fig. 1(a). The Maxwell equation $\nabla \times \mathbf{E} = -\frac{1}{c}\frac{\partial \mathbf{B}}{\partial t}$ infers the corresponding magnetic field to be $\mathbf{B} = -\mathbf{e}_x E_0 \cos ky \sin\omega t$, suggesting the spatial function is a quarter of the wavelength λ out of phase, which introduces different spatial dependences for the $E1$ and $M1$ interactions. Moreover, as the $E2$

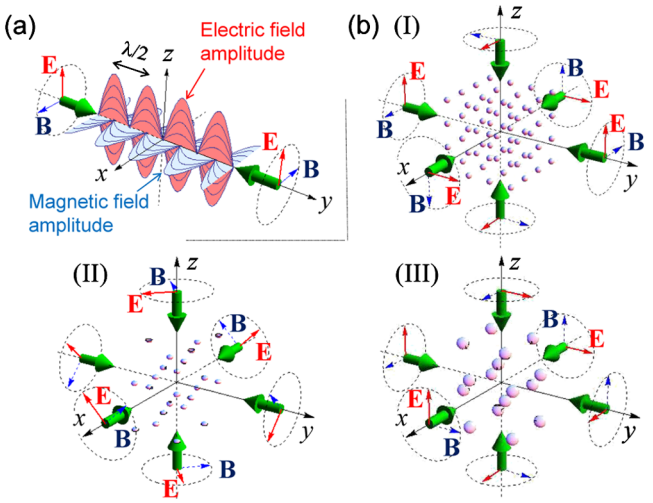

FIG. 1 (color online). (a) Spatial distribution of an electromagnetic field for a 1D standing wave. (b) Configuration of the electromagnetic fields and optical lattices for cases (I)–(III), as described in the text. Optical lattice sites inside $|x|, |y|, |z| < 0.9\lambda$ are indicated with their equipotential surfaces given by $q_{E1}(\mathbf{r}) = 0.3$ and $\rho_\xi = 1$.

interaction is proportional to the electric field gradient, its spatial dependence also differs from that of $E1$. These different spatial dependences do not allow perfect cancellation of the quadratic light shift in the clock transitions [13]. However, by admitting a constant differential light shift offset, we will show that the spatial mismatch of the light shift can be eliminated; therefore, the atomic-motion-dependent clock shift, which is detrimental to atomic clocks, can be removed.

As there are hyperpolarizability effects [2,8] that cannot be moderated by the magic wavelength, a blue-detuned magic wavelength that confines atoms near the nodes of standing waves would be a promising choice, which will reduce the relevant uncertainties down to 2×10^{-19} [14]. Although the local electric field intensity for atoms is reduced, the $E2$ interaction, in turn, may severely affect the accuracy of a blue-detuned lattice clock, as the electric field gradient can generally be maximum at the nodes of the standing wave.

We consider 3D optical lattices consisting of three mutually orthogonal standing waves, whose results are straightforwardly applicable to lower dimensional lattices such as red-detuned 1D lattices. In particular, we derive spatial dependences $q_X(\mathbf{r})$ of the quadratic light shift with $X = E1$, $M1$, and $E2$ interactions. For generality, we assume electric field amplitudes $E_\xi = \rho_\xi E_0$ of the three standing waves and polarization vectors $\mathbf{p}_\xi$ and $\mathbf{p}_\xi^b$ ($|\mathbf{p}_\xi| = |\mathbf{p}_\xi^b| = 1$) for the forward and backward running waves, respectively, in the $\xi = x, y, z$ directions denoted by unit vectors $\mathbf{e}_\xi$:

$$\begin{aligned}\mathbf{E}_\xi(\xi, t) &= E_\xi[\mathbf{p}_\xi \cos(k\xi - \omega t) + \mathbf{p}_\xi^b \cos(k\xi + \omega t)] \\ &= E_\xi(\mathbf{p}_\xi^+ \cos k\xi \cos\omega t + \mathbf{p}_\xi^- \sin k\xi \sin\omega t), \quad (1)\end{aligned}$$

where we define $\mathbf{p}_\xi^\pm \equiv \mathbf{p}_\xi \pm \mathbf{p}_\xi^b$. The total electric field vector in this lattice is given by $\mathbf{E}(\mathbf{r}, t) = \sum_{\xi=x,y,z} \mathbf{E}_\xi(\xi, t)$.

The principal contribution to the lattice potential is given by the second-order quasienergy shift due to the electric dipole atom-field interaction $\hat{V}_{E1}(\mathbf{r}, \mathbf{r}_e, t) = -\mathbf{d} \cdot \mathbf{E}(\mathbf{r}, t)$ [15],

$$\begin{aligned}U_{E1}(\mathbf{r}) &= -\langle\langle \psi | \hat{V}_{E1} \mathcal{G}(\mathbf{r}_e, t; \mathbf{r}_e', t') \hat{V}_{E1} | \psi \rangle\rangle \\ &= -\frac{E_0^2}{2} \alpha_{E1}(\omega) q_{E1}(\mathbf{r}), \quad (2)\end{aligned}$$

where $\mathbf{r}_e$ is the position vector of the outermost atomic electron relative to the atomic nucleus at $\mathbf{r}$, $\mathbf{d} = -\mathbf{r}_e$ is the electric dipole moment, and $\mathcal{G}(\mathbf{r}_e, t; \mathbf{r}_e', t')$ is the quasienergy Green function of an atom. Here the atomic units are used, $e = m = \hbar = 1$, where the speed of light is $c \approx 137$. The double angular brackets in Eq. (2) denote the time integration (in variables t and t') over the field oscillation period $T = 2\pi/\omega$ and the spatial integration over the position $\mathbf{r}_e$ of the atomic electron. With the use of the electric field in Eq. (1), the spatial distribution function of the atom-field $E1$ interaction energy is given by

$$q_{E1}(\mathbf{r}) = \frac{1}{2}\left(\sum_\xi \rho_\xi \mathbf{p}_\xi^+ \cos k\xi\right)^2 + \frac{1}{2}\left(\sum_\xi \rho_\xi \mathbf{p}_\xi^- \sin k\xi\right)^2. \quad (3)$$

To evaluate the contribution of the $M1$ interaction, it is sufficient to determine the magnetic field component of the lattice, which for each running wave with wave vector $\mathbf{k}_\xi$ is given by $\mathbf{B}_\xi(\mathbf{r}, t) = \mathbf{k}_\xi/k \times \mathbf{E}_\xi(\mathbf{r}, t)$. The total magnetic field corresponding to the electric field in Eq. (1) is given by,

$$\begin{aligned}\mathbf{B}(\mathbf{r}, t) = \sum_{\xi=x,y,z} E_\xi(&\mathbf{e}_\xi \times \mathbf{p}_\xi^+ \sin k\xi \sin\omega t + \mathbf{e}_\xi \\ &\times \mathbf{p}_\xi^- \cos k\xi \cos\omega t). \quad (4)\end{aligned}$$

The magnetic dipole contribution to the lattice potential may be written similarly to Eq. (2), as the quasienergy shift corresponding to the atom-field $M1$ interaction is described by the Hamiltonian $\hat{V}_{M1} = -\hat{\mathbf{m}} \cdot \mathbf{B}(\mathbf{r}, t)$, where $\hat{\mathbf{m}} = -(\hat{\mathbf{J}} + \hat{\mathbf{S}})/2c$ is the magnetic moment of an atom with atomic total momentum $\mathbf{J}$ and spin $\mathbf{S}$. The spatial distribution of the $M1$ interaction is given by,

$$\begin{aligned}q_{M1}(\mathbf{r}) = &\frac{1}{2}\left(\sum_\xi \rho_\xi \mathbf{e}_\xi \times \mathbf{p}_\xi^+ \sin k\xi\right)^2 \\ &+ \frac{1}{2}\left(\sum_\xi \rho_\xi \mathbf{e}_\xi \times \mathbf{p}_\xi^- \cos k\xi\right)^2. \quad (5)\end{aligned}$$

In the nonrelativistic approximation, the magnetic dipole polarizability in the n^1S_0 ground state is zero, while for the n^3P_0 metastable state, it is given by

$$\alpha_{M1}(\omega) = \frac{E_{n^3P_1} - E_{n^3P_0}}{6c^2[(E_{n^3P_1} - E_{n^3P_0})^2 - \omega^2]}, \quad (6)$$

which is evidently the value of the second order in the fine-structure constant $\alpha = 1/c$. $\alpha_{M1}(\omega)$ remains negative for ω higher than the $n^3P_0 - n^3P_1$ transition frequency.

Not less important than the $M1$ Stark shift may be the contribution of the electric quadrupole ($E2$) interaction,

$$\begin{aligned}U_{E2}(\mathbf{r}) &= -\langle\langle \psi | \hat{V}_{E2} \mathcal{G}(\mathbf{r}_e, t; \mathbf{r}_e', t') \hat{V}_{E2} | \psi \rangle\rangle \\ &= -\frac{E_0^2}{2} \alpha_{E2}(\omega) q_{E2}(\mathbf{r}). \quad (7)\end{aligned}$$

The value of the quadrupole polarizability $\alpha_{E2}(\omega)$ is of the second order in α, just as the magnetic dipole polarizability in Eq. (6). The $E2$ interaction operator may be taken from the Taylor series in powers of the small parameter $k|\mathbf{r}_e| \ll 1$ for the total atom-electric-field interaction Hamiltonian,

$$\hat{V}_E(\mathbf{r}, \mathbf{r}_e, t) = \mathbf{r}_e \cdot \sum_{s=0}^{\infty} \frac{(\mathbf{r}_e \cdot \nabla)^s}{(s+1)!} \mathbf{E}(\mathbf{r}, t), \quad (8)$$

where all derivatives are taken with respect to the components of the position vector $\mathbf{r}$, while $\mathbf{r}_e$ is assumed constant. $\hat{V}_E(\mathbf{r}, \mathbf{r}_e, t)$ includes all higher-order multipole interactions: The $s = 0$ term corresponds to the Hamiltonian

$\hat{V}_{E1}(\mathbf{r}, t)$ and the $s = 1$ term to the Hamiltonian $\hat{V}_{E2}(\mathbf{r}, t)$. After substitution of this operator into Eq. (7) and integration over time and angular variables, the spatial distribution of the quadrupole energy is determined:

$$q_{E2}(\mathbf{r}) = \frac{1}{2}\sum_{(\xi,\eta)} (\rho_\xi \mathbf{e}_\eta \cdot \mathbf{p}_\xi^+ \sin k\xi + \rho_\eta \mathbf{e}_\xi \cdot \mathbf{p}_\eta^+ \sin k\eta)^2 + \frac{1}{2}\sum_{(\xi,\eta)} (\rho_\xi \mathbf{e}_\eta \cdot \mathbf{p}_\xi^- \cos k\xi + \rho_\eta \mathbf{e}_\xi \cdot \mathbf{p}_\eta^- \cos k\eta)^2, \tag{9}$$

where the sum runs over $(\xi, \eta) = (x, y)$, (y, z), and (z, x). Correspondingly, the quadrupole polarizabilities of the ground and excited states are written in terms of the radial matrix elements, e.g., for the $|\psi\rangle = |n^1S_0\rangle$ state,

$$\alpha_{E2}^{^1S_0}(\omega) = \frac{\omega^2}{60c^2}\langle n^1S_0|r_e^2(g_{^1D_2}^{\omega} + g_{^1D_2}^{-\omega})r_e^2|n^1S_0\rangle, \tag{10}$$

where the radial Green functions $g_{^1D_2}^{\pm\omega}$ of the singlet D-state subspace appear.

Below we illustrate a few representative examples that allow cancellation of spatial mismatch of the lattice potentials. They are assorted by the electric field $\mathbf{E}_f$ and $\mathbf{E}_b$ of the forward and backward running waves that compose lattice standing waves, as summarized in Fig. 1(b). (I) $\mathbf{E}_f \parallel \mathbf{E}_b$ standing waves ($\mathbf{p}_\xi = \mathbf{p}_\xi^b$), in which we take $\mathbf{p}_x = \mathbf{e}_y$, $\mathbf{p}_y = \mathbf{e}_z$, and $\mathbf{p}_z = \mathbf{e}_x$. The $E1$ distribution is calculated to be

$$q_{E1}(\mathbf{r}) = 2(\rho_x^2\cos^2 kx + \rho_y^2\cos^2 ky + \rho_z^2\cos^2 kz). \tag{11}$$

The $M1$ and $E2$ distributions are given by

$$q_{M1}(\mathbf{r}) = q_{E2}(\mathbf{r}) = \Delta q - q_{E1}(\mathbf{r}), \tag{12}$$

with $\Delta q = 2(\rho_x^2 + \rho_y^2 + \rho_z^2)$. Thus the distributions of $M1$ and $E2$ shifts in this lattice coincide and differ from $q_{E1}(\mathbf{r})$ in sign and by a constant offset of Δq. (II) $\mathbf{E}_f \perp \mathbf{E}_b$ standing waves ($\mathbf{p}_\xi \perp \mathbf{p}_\xi^b$) with their polarization vectors pointing at an angle $\pi/4$ to the standing-wave beams, i.e., $\mathbf{p}_x = (\mathbf{e}_y + \mathbf{e}_z)/\sqrt{2}$, $\mathbf{p}_x^b = (-\mathbf{e}_y + \mathbf{e}_z)/\sqrt{2}$, $\mathbf{p}_y = (\mathbf{e}_z + \mathbf{e}_x)/\sqrt{2}$, $\mathbf{p}_y^b = (-\mathbf{e}_z + \mathbf{e}_x)/\sqrt{2}$, $\mathbf{p}_z = (\mathbf{e}_x + \mathbf{e}_y)/\sqrt{2}$, and $\mathbf{p}_z^b = (\mathbf{e}_x - \mathbf{e}_y)/\sqrt{2}$. The $E1$ and $E2$ distributions here coincide and $M1$ differs from them by sign and an offset,

$$\begin{aligned} q_{E1}(\mathbf{r}) &= q_{E2}(\mathbf{r}) \\ &= \Delta q/2 + 2\rho_x\rho_z \sin kx \sin kz \\ &\quad + 2\rho_y\rho_z \cos ky \cos kz, \\ q_{M1}(\mathbf{r}) &= \Delta q - q_{E1}(\mathbf{r}). \end{aligned} \tag{13}$$

(III) $\mathbf{E}_f \perp \mathbf{E}_b$ standing waves ($\mathbf{p}_\xi \perp \mathbf{p}_\xi^b$), in which we take polarization vectors to be $\mathbf{p}_x^\pm = \mathbf{e}_y \pm \mathbf{e}_z$, $\mathbf{p}_y^\pm = \mathbf{e}_z \pm \mathbf{e}_x$, and $\mathbf{p}_z^\pm = \mathbf{e}_x \pm \mathbf{e}_y$. Then the $E1$ and $M1$ distributions coincide and $E2$ differs from them by sign and an offset,

$$\begin{aligned} q_{E1}(\mathbf{r}) &= q_{M1}(\mathbf{r}) \\ &= \Delta q/2 + \rho_x\rho_y \cos k(x + y) \\ &\quad + \rho_y\rho_z \cos k(y + z) + \rho_z\rho_x \cos k(z + x), \\ q_{E2}(\mathbf{r}) &= \Delta q - q_{E1}(\mathbf{r}). \end{aligned} \tag{14}$$

As indicated by these examples, it is essential that the spatial distributions of $q_X(\mathbf{r})$ may show the same spatial dependences apart from the sign and an offset Δq for particular lattice geometries. However, we note that this is not a general feature for optical lattices. For example, in the 3D lattice with $\mathbf{E}_f \parallel \mathbf{E}_b$, standing waves with $\mathbf{p}_x = \mathbf{p}_y = \mathbf{e}_z$, and $\mathbf{p}_z = \mathbf{e}_x$ employed in our previous experiment [16], neither $q_{M1}(\mathbf{r})$ nor $q_{E2}(\mathbf{r})$ shows the same spatial dependencies as $q_{E1}(\mathbf{r})$; therefore, the motional effects may limit clock uncertainties in future experiments.

These three examples show prominent features by themselves. For a magic frequency, where the $E2$ ($M1$) interaction is significantly larger than the $M1$ ($E2$) interaction, case (II) [case (III)] will be more advantageous than the others, as the less significant $M1$ ($E2$) contribution may well be neglected. For application to the blue magic wavelength, which highlights the reduction of the hyperpolarizability effects by trapping atoms near the nodes, case (I) would be a reasonable choice, as Eq. (11) suggests the creation of perfect nodes regardless of the intensity balance in the orthogonal lattice beams. Regarding the lattice light polarization, case (I) shows linear polarization, while cases (II) and (III) have elliptical polarizations that may give rise to the vector shift for atoms with nonzero angular momentum.

Hereafter, we focus on case (I) and consider its application to the blue-detuned magic wavelength. The clock transition frequency is expressed as

$$\nu_{\text{clock}}(\omega) = \nu_0 - \tfrac{1}{2}\Delta\alpha_{\text{EM}}(\omega)q_{E1}(\mathbf{r})E_0^2 - \tfrac{1}{2}\Delta\alpha_0(\omega)\Delta q E_0^2 + \mathcal{O}(E_0^4), \tag{15}$$

where ν_0 is the atomic transition frequency. The quadratic light shift is decomposed into a spatially modulated and uniform terms by $\Delta\alpha_{\text{EM}}(\omega) \equiv \Delta\alpha_{E1}(\omega) - \Delta\alpha_0(\omega)$ and $\Delta\alpha_0(\omega) \equiv \Delta\alpha_{M1}(\omega) + \Delta\alpha_{E2}(\omega)$ using differential $E1$, $M1$, and $E2$ polarizabilities in the clock transition. Besides the hyperpolarizability effects that are minimized by use of a blue-detuned lattice, the magic frequency ω_m may be given by $\Delta\alpha_{\text{EM}}(\omega_m) = 0$ [17], allowing us to define ω_m independent of atomic motional states. The residual $M1$-$E2$ term $\delta\nu = -\frac{1}{2}\Delta\alpha_0(\omega_m)\Delta q E_0^2$ provides an atomic-position-independent offset, which is solely related to the total lattice laser intensity $\Delta q E_0^2 = 2(E_x^2 + E_y^2 + E_z^2)$.

To find the magic frequency experimentally, the atomic-motion-dependent term in Eq. (15) needs to be discriminated. Harmonically approximating the trapping potential near the lattice node, e.g., at $x = y = z = \lambda/4$ and averaging over the atom positions in the oscillator state

$|\mathbf{n}\rangle = |n_x, n_y, n_z\rangle$, the second term in the right-hand side of Eq. (15) should be replaced by

$$2\left\langle -\frac{1}{2}\Delta\alpha_{\mathrm{EM}} q_{E1}(\mathbf{r}) E_0^2 \right\rangle_{\mathbf{n}} = \sum_{\xi} (\Omega_\xi^P - \Omega_\xi^S)\left(n_\xi + \frac{1}{2}\right), \tag{16}$$

where $\Omega_\xi^{(\ell)} = k\rho_\xi E_0 \sqrt{2|\alpha_{\mathrm{EM}}^{(\ell)}(\omega)|/\mathcal{M}}$ is the vibrational frequency of atoms in the ξ direction of the lattice potential for the $\ell = P(^3P_0)$ or $S(^1S_0)$ state. Here $\mathcal{M}$ is the mass of the atom, $\alpha_{\mathrm{EM}}^{(\ell)}(\omega) \equiv \alpha_{E1}^{(\ell)}(\omega) - \alpha_{M1}^{(\ell)}(\omega) - \alpha_{E2}^{(\ell)}(\omega)$ is given by the $E1$, $M1$, and $E2$ polarizabilities in the ℓ state, and factor 2 accounts for the kinetic energy.

The magic frequency ω_m can be determined by measuring the atomic-motion-dependent clock shift $\Delta\nu(\omega, \delta\mathbf{n}) = \nu_{\mathrm{clock}}(\omega, \delta\mathbf{n} + \mathbf{n}) - \nu_{\mathrm{clock}}(\omega, \mathbf{n})$ for atoms occupying vibrational states differing by $\delta\mathbf{n}$ and minimizing it to be zero, i.e., $\Delta\nu(\omega_m, \delta\mathbf{n}) = 0$, rather than by investigating the lattice intensity dependent clock shift [18,19]. Once the magic frequency is determined, the residual $M1$-$E2$ offset $\delta\nu$ can be evaluated by the vibrational frequencies $\Omega_\xi = \Omega_\xi^S(\omega_m) = \Omega_\xi^P(\omega_m)$ of the lattice potential as

$$\delta\nu = -\frac{\mathcal{M}\Delta\alpha_0}{2k^2|\alpha_{\mathrm{EM}}|}(\Omega_x^2 + \Omega_y^2 + \Omega_z^2). \tag{17}$$

Therefore all the essential measurements are done by the frequency measurements, once the magic frequency or wavelength is measured and shared. The same strategy should apply to 1D optical lattices with red-detuned magic wavelength by setting $\rho_x \neq 0$ and $\rho_y = \rho_z = 0$ in case (I).

The proposed optical lattice will be conveniently realized by a folded lattice [16,21], which maintains the relative phases of the orthogonal standing waves to realize linear lattice polarizations. Equation (1) assumes that the intensities of the counter-propagating beam pairs are balanced, which is accomplished by preparing lattice beams inside an optical cavity [16]. The blue-detuned magic wavelength for the Sr clock transition is experimentally determined to be $\lambda_m = 2\pi c/\omega_m \approx 389.9$ nm [14], where the numerical estimates for this lattice give $\Delta\alpha_0/|\alpha_{\mathrm{EM}}| \approx -1.4 \times 10^{-7}$ with $\Delta\alpha_{M1}/\Delta\alpha_{E2} \approx 8 \times 10^{-3}$ [22]. Therefore, the offset frequency is given by $\delta\nu/2\pi \approx 40I$ mHz for a trap frequency of $\Omega_\xi/2\pi = 75\sqrt{I}$ kHz, where I is the single running wave laser intensity measured in kW/cm^2 assuming $\rho_\xi = 1$. The uncertainty for this correction may be evaluated to be $\approx 4I$ mHz, assuming an inhomogeneity of the lattice intensity of 10%.

For ^{87}Sr atoms with a total angular momentum of $F = 9/2$, the tensor light shift due to the spatial rotation of the lattice polarization with respect to the quantization axis may occur. As the shift is proportional to the light intensity near the nodes, the shift may be reduced to the mHz level for the blue magic wavelength. Bosonic isotopes such as ^{88}Sr or other atomic elements with nuclear spin of $I = 1/2$, e.g., ^{171}Yb or ^{199}Hg may well be used to suppress the tensor light shift.

In summary, we present general formulas for the quadratic light shift taking multipolar atom-field interactions into account and show that the spatial mismatch of the interactions in the clock transition can be treated as a spatially constant offset $\delta\nu$ for specific lattice geometries. Numerical estimates are made for Sr atoms, and the relevant correction can be determined by trap frequency measurements with the mHz level. Combined with the blue magic wavelength, the hyperpolarizability effect is minimized as it solely contributes to the anharmonic part of the space-dependent light shift and clock uncertainty at the 10^{-18} level will be within reach.

This work was supported by the Photon Frontier Network Program, MEXT, Japan, and by the Russian Foundation for Basic Research (RFBR Grant No. 07-02-00279a). H. K. acknowledges M. Takamoto for useful comments.

[1] H. G. Dehmelt, IEEE Trans. Instrum. Meas. **IM-31**, 83 (1982).
[2] H. Katori, M. Takamoto, V. G. Pal'chikov, and V. D. Ovsiannikov, Phys. Rev. Lett. **91**, 173005 (2003).
[3] T. Rosenband *et al.*, Science **319**, 1808 (2008).
[4] A. D. Ludlow *et al.*, Science **319**, 1805 (2008).
[5] N. Yu, X. Zhao, H. Dehmelt, and W. Nagourney, Phys. Rev. A **50**, 2738 (1994).
[6] W. M. Itano, J. Res. Natl. Inst. Stand. Technol. **105**, 829 (2000).
[7] A. V. Taichenachev *et al.*, Phys. Rev. Lett. **96**, 083001 (2006).
[8] A. Brusch *et al.*, Phys. Rev. Lett. **96**, 103003 (2006).
[9] G. P. Barwood *et al.*, Phys. Rev. Lett. **93**, 133001 (2004).
[10] P. Dubé *et al.*, Phys. Rev. Lett. **95**, 033001 (2005).
[11] C. F. Roos *et al.*, Nature (London) **443**, 316 (2006).
[12] T. Schneider, E. Peik, and C. Tamm, Phys. Rev. Lett. **94**, 230801 (2005).
[13] A. V. Taichenachev *et al.*, Phys. Rev. Lett. **101**, 193601 (2008).
[14] M. Takamoto *et al.*, Phys. Rev. Lett. **102**, 063002 (2009).
[15] N. L. Manakov, V. D. Ovsiannikov, and L. P. Rapoport, Phys. Rep. **141**, 320 (1986).
[16] T. Akatsuka, M. Takamoto, and H. Katori, Nature Phys. **4**, 954 (2008).
[17] This definition of the magic frequency is different from that in Ref. [14] determined for a traveling wave.
[18] M. Takamoto, F.-L. Hong, R. Higashi, and H. Katori, Nature (London) **435**, 321 (2005).
[19] The spectral line broadening due to the thermal vibrational state occupation was used to determine the magic wavelength in Ref. [20].
[20] M. Takamoto and H. Katori, Phys. Rev. Lett. **91**, 223001 (2003).
[21] A. Rauschenbeutel, H. Schadwinkel, V. Gomer, and D. Meschede, Opt. Commun. **148**, 45 (1998).
[22] As for the red-detuned lattice at $\lambda_m \approx 813.4$ nm, $\Delta\alpha_0/|\alpha_{\mathrm{EM}}| \approx -3.3 \times 10^{-8}$ with $\Delta\alpha_{M1}/\Delta\alpha_{E2} \approx 7 \times 10^{-2}$.